energies

MDPI

*Article*

# A Novel Intelligent Fan Clutch for Large Hybrid Vehicles

**Ruizhi Shu, Hang Gong, Guanghui Hu and Jin Huang ***

Department of Mechanical Engineering, Chongqing University of Technology, Chongqing 400054, China; ruizhishu@cqut.edu.cn (R.S.); GongHang@stu.cqut.edu.cn (H.G.); huguanghui@stu.cqut.edu.cn (G.H.)
* Correspondence: jhuangcq@cqut.edu.cn

**Abstract:** To solve the problems of complex structure, poor reliability, and low intelligence of existing fan clutches for large hybrid vehicles, this paper proposes a new adaptive shape memory alloy intelligent fan clutch for large hybrid vehicle motor cooling. Based on the pure shear shape memory alloy thermodynamic effects, the relationship between shape memory alloy spring recovery force and temperature has been established; based on the shape memory alloy spring thermal drive characteristics and clutch construction dimensions, clutch torque transmission equations have been established. The shape memory alloy fan clutch transmission characteristics were quantitatively analyzed in terms of temperature, torque, rotational speed, and slip rate. The results show that the shape memory alloy fan clutch model based on the finite element method (FEM) and the established transmission model can accurately describe the mechanical characteristics of the shape memory alloy phase change process and the clutch torque transmission characteristics. When the clutch input speed is 3000 rad/min and the temperature is 100 °C, the output torque is 19.04 N·m, the speed is 2877.2 rad/min, and the slip rate is 4.3%. Due to the shape memory effect of shape memory alloy, the clutch can intelligently adjust the fan speed by sensing the ambient temperature. A fan clutch can satisfy the heat dissipation requirement of a large hybrid vehicle's transmission system under complicated road conditions.

**Keywords:** shape memory alloys; fan clutches; temperature; transmission performance; thermal performance

**Citation:** Shu, R.; Gong, H.; Hu, G.; Huang, J. A Novel Intelligent Fan Clutch for Large Hybrid Vehicles. *Energies* **2022**, *15*, 4308. https://doi.org/10.3390/en15124308

Academic Editors: Minghui Hu, Changzhao Liu and Chunyun Fu

Received: 24 May 2022
Accepted: 9 June 2022
Published: 12 June 2022

**Publisher's Note:** MDPI stays neutral with regard to jurisdictional claims in published maps and institutional affiliations.



## 1. Introduction

Shape memory alloys (SMAs) are a new class of intelligent alloy materials with shape memory effect and super elasticity [1,2]. The excellent shape memory effect is demonstrated by the fact that the internal structure of SMAs can complete the reversible transformation from non-twinning low-temperature martensite to high-temperature austenite when the working temperature of SMA changes, and the external morphology of SMA changes accordingly to the internal structure of the crystal [3,4]. SMA has a unique shape memory effect and super elasticity; based on this, shape-memory-effect-made components have the advantages of intelligence and controllability [5,6]. Shape memory alloy is a typical intelligent material that can convert thermal energy into mechanical energy. Shape memory alloy has a wide range of applications in automotive transmission, mechanical control energy management strategies, and transmission [7–9]. Imran Husam Yahya et al. [10] used shape memory alloys in automotive temperature sensors to automatically sense the temperature of an automotive engine using the ability of shape memory alloys to shrink at different temperatures. Venkata Siva C Chillara et al. [11] used shape memory alloys in automotive fenders by coupling shape memory alloys with integrated quick-release latches, resulting in a 95% reduction in conventional latch actuation time and a 62% reduction in shape memory alloy fender mass compared to conventional fenders. Shivaram et al. [12] used shape memory alloys to improve the stiffness of automotive suspensions, which can improve the performance of a car without compromising

ride comfort. All the above-mentioned use the temperature-sensitive properties of shape memory alloys as automotive sensors and actuators, respectively, which greatly improves the energy efficiency of automobiles. However, the sensing, response, and driving characteristics have not been combined to develop the corresponding intelligent actuators.

At present, in order to solve the problem of the hybrid vehicle transmission system in the work process due to heat leading to a sharp decline in transmission performance, the basic method of cooling the system of transmission is used in order to protect the power unit, to maintain the power system in optimal working condition while improving the economy of the fuel engine and battery safety. Most hybrid energy vehicles today use (electronically controlled) silicone oil clutches or electromagnetic clutches to control the rotation of the cooling fan. These switch-type clutches can only combine or disengage the clutch at a specific temperature and cannot adapt to the cooling requirements at various temperatures [13,14]. An electromagnetic clutch can be electronically controlled to achieve multi-stage speed control, but with the introduction of additional control devices to reduce the reliability of the clutch, the structure is more complex, and for some hybrid vehicles in harsh environmental conditions, the traditional electromagnetic clutch struggles to ensure the stability of the work of the transmission system [15,16]. Based on this, in order to solve the defects of complex clutch structure, low reliability, and high power consumption in the transmission system of hybrid vehicles [17,18], in this paper, an intelligent fan clutch based on the shape memory effect of SMAs is proposed. The nonlinear friction torque generated by an SMA spring under thermal drive enables the clutch to have good transmission characteristics under any temperature of hybrid vehicles, and the self-adaptive nature of the clutch under different temperatures can realize intelligent speed regulation of the fan, solve the problems such as serious heating of the transmission system, and can significantly reduce energy consumption and improve the stability of the transmission system. The theoretical analysis and experiment provide the basis for the design and manufacture of an SMA intelligent fan clutch.

## 2. Working Principle

The schematic diagram of the structure of the intelligent SMA fan clutch for a large hybrid vehicle engine is shown in Figure 1. The main parts of the clutch are (1) drive shaft, (2) clutch housing, (3) drive disc, (4) SMA spring, (5) friction slide, and (6) friction ring. The SMA fan clutch operates as follows:

(1) When the ambient temperature is lower than the austenite transformation temperature of the SMA, the SMA does not produce the shape memory effect and cannot drive the friction slider to produce friction torque, so the clutch is disengaged in this state and the active shaft cannot drive the clutch housing to rotate.

(2) When the ambient temperature reaches the austenite transformation temperature of the SMA and the temperature continues to rise, the SMA starts to produce the shape memory effect and the SMA spring starts to elongate and drive the friction slider and the friction ring to produce friction torque. The flow vanes on the drive disk draw hot air into the clutch, allowing the SMA spring to quickly sense the ambient temperature through forced convection. As the temperature increases, the frictional torque generated by the SMA spring increases, and when the temperature reaches the SMA's austenite end transition temperature, the torque transmitted by the clutch reaches its maximum.

(3) When the clutch temperature drops to the martensite transformation temperature of the SMA and continues to decrease, the SMA spring begins to contract and the frictional torque begins to decrease due to the bidirectional shape memory effect of the SMA. When the temperature decreases to the end of the martensite transformation temperature of the SMA, no friction torque is generated between the friction slider and the friction ring, and the clutch returns to the disengaged state.

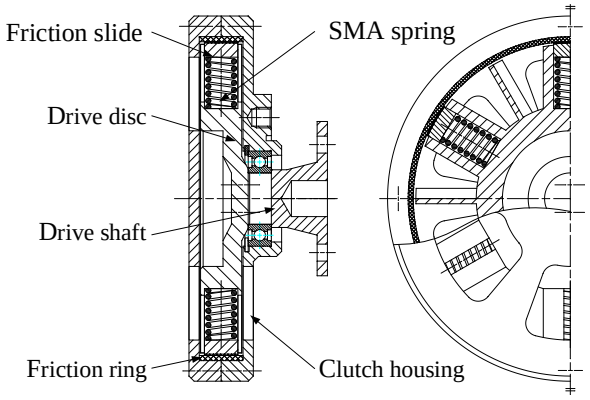


**Figure 1.** Schematic diagram of adaptive SMA fan clutch.

## 3. Theoretical Model

### *3.1. Thermodynamic Model of Pure Shear SMA*

The critical temperatures of SMA in the stress-free state are $M_s$, $M_f$, $A_s$, and $A_f$ (martensitic phase transformation start temperature, martensitic phase transformation end temperature, austenitic phase transformation start temperature, and austenitic phase transformation end temperature). The thermodynamic process of the shape memory effect of an SMA can be accurately described by the shape memory factor $\eta(\eta \in (0,1))$. During the loading process of an SMA, the SMA starts to generate recoverable nonlinear strain, and the shape memory factor $\eta$ increases from 0 to 1 with the gradual increase of load when the recoverable nonlinear strain generated by SMA reaches the maximum value. The shape memory factor and recoverable nonlinear strain do not change during the SMA unloading process. When the SMA is heated after unloading, the SMA transforms from non-twin martensite to austenite. When the SMA reaches the critical temperature, the shape memory factor decreases gradually with temperature, and the recoverable nonlinear strain of the SMA gradually recovers. Combined with the microscopic mechanism of SMA, the relationship between the shape memory factor $\eta$ and the volume fraction $\xi$ of martensite can be expressed as [19]

$$\xi = \xi_0 + (1 - \xi_0)\eta \tag{1}$$

where $\eta$ is the shape memory factor, $\xi$ is the volume fraction of martensite, and $\xi_0$ is initial value of $\xi$.

Assuming a linear relationship between the shape memory factor $\eta$ and the shear stress and temperature, the relationship between the shape memory factor $\eta$ and the shear stress $\tau$ and temperature during the unloading of SMA in pure shear can be derived from the relationship between the phase change critical stress and temperature as

$$\eta = \eta_{u0}\frac{\tau - \tau_{A_f}}{\tau_{A_s} - \tau_{A_f}} \tag{2}$$

where $\tau$ is shear stress, $\tau_{A_s}$ and $\tau_{A_f}$ are the shear stress at the beginning of austenite and the shear stress at the end of austenite, and $\eta_{u0}$ is the initial value of shape memory alloy factor during the process of unloading, respectively.

Assuming that SMA is isotropic, when SMA is in pure shear state, the three-dimensional meso-mechanical constitutive equation of SMA in pure shear mode can be simplified as [20]

$$\gamma = \frac{\tau}{G(\xi)} + \frac{\sqrt{6}}{2}\varepsilon_L\eta \tag{3}$$

where $\varepsilon_L$ is maximum residual strain and $G(\xi)$ is SMA shear modulus. It can be expressed as

$$G(\xi) = \frac{E}{2(1+\nu)} = G_A + (G_M - G_A)\xi \quad (4)$$

where $G_A$ and $G_M$ are the shear moduli of martensite and austenite, and $E$ and $\nu$ are the elastic modulus and Poisson's ratio of SMA.

$$\gamma = \frac{\tau}{G(\xi)} + \frac{\tau_0}{G(\xi_0)} + \frac{\sqrt{6}}{2}\varepsilon_L(\eta - \eta_{u0}) + \gamma_0 \quad (5)$$

where $G(\xi_0)$ is the initial value of SMA shear modulus, $\tau_0$ is the initial value of shear stress, and $\gamma_0$ is the cut strain.

### *3.2. Torque Characteristics of SMA Fan Clutch*

The direction of the force during spring loading of SMA helices was always along the axis of the spring, so SMA filaments were always subjected to pure shear load. When $x$ is the center to the outer edge of the section, the linear shear strain of the SMA filament section can be expressed as [21]

$$\gamma = \theta x \; x \in (0, r) \quad (6)$$

where $\theta$ is the torsion angle of the SMA wire and $r$ is the radius of the SMA wire.

When the diameter of the spring is $D(D = 2R)$ and the number of effective coils is $n$, the axial deformation of the spring can be expressed as

$$f = \frac{\pi n \theta D^2}{2} = 2\pi n \theta R^2 \quad (7)$$

where $R$ is the radius of the spring.

Combining Equations (5) and (6), the relationship between the twisting angle of SMA wire and the shear stress in the section is obtained as [22]

$$\gamma_s = \theta\frac{d}{2} = \frac{\tau}{G(\xi)} + \frac{\tau_0}{G(\xi_0)} + \frac{\sqrt{6}}{2}\varepsilon_L(\eta - \eta_0) + \gamma_0 \quad (8)$$

where $d$ is the SMA wire diameter.

Combining Equation (7) with Equation (8), the SMA coil spring axial deformation $f$ is [23]

$$f = \frac{\pi n D^2}{d}\left(\frac{\tau}{G(\xi)} + \frac{\tau_0}{G(\xi_0)} + \frac{\sqrt{6}}{2}\varepsilon_L(\eta - \eta_0) + \gamma_0\right) \quad (9)$$

where $\tau$ is the shear stress of the SMA wire section, and the shear stress of the coil spring can be expressed as

$$\tau = k\frac{8FD}{\pi d^3} \quad (10)$$

where the axial load is $F$, $d$ represents the wire diameter, $C$ is the spring index, $C = D/d$, and $\kappa$ is known as the Wahl correction factor applied:

$$k = \frac{4C-1}{4C-4} + \frac{0.615}{C} \quad (11)$$

where $C$ is the coiling ratio of the coil spring (C = D/d).

Combining Equations (8) and (9), the axial displacement $f$ produced by the SMA coil spring under the axial load $F$ is derived as [24]

$$f = k\frac{8nFD^3}{d^4 G(\xi)} - \frac{\pi n D^2}{d}\beta \quad (12)$$

where k is the stress correction factor and $\beta$ is the intermediate variable, calculated as

$$\beta = \frac{\tau_0}{G(\xi_0)} + \frac{\sqrt{6}}{2}\varepsilon_L(\eta - \eta_0) + \gamma_0 \tag{13}$$

Organizing Equation (12) yields that the recovery force $F_r$ generated by the SMA helical spring is

$$F_r = \frac{d^4 G(\xi)}{8knD^3} f + \frac{\pi d^3 G(\xi)}{8kD}\beta \tag{14}$$

When SMA springs drive the slider to contact with the friction ring, the friction torque can be expressed as

$$M_f = N\mu F_r R_e \tag{15}$$

where $N$ is the number of slides driven by the SMA spring, $\mu$ is the friction coefficient between the slider and the friction ring, and $R_e$ is the radius at the contact friction.

As the clutches' output shaft attached fans turn, the workload resulting from air resistance can be expressed as

$$M_c = K_a \rho \left(\frac{D}{1000}\right)^5 n_p^2 \tag{16}$$

where $K_a$ is the torque coefficient in air, $\rho$ is the air density, $D$ is the fan blade diameter, and $n_p$ is the fan speed. When the friction torque $M_f$ generated by the clutch is balanced with the work load $M_c$ generated by the fan, the fan speed $n_p$ can be derived by Equation (16).

## 4. Clutch FEM Analysis

In order to verify the accuracy of the theoretical model in Chapter 3, analysis of the model was carried out by the finite element method. The FEM is able to analyze and simulate the nonlinear thermodynamic properties of SMA springs in different states of SMA during the phase change process and analyze the transmission performance of the SMA fan clutch. The FEM analysis process is as follows: First, the SMA thermodynamic intrinsic model in pure shear mode shown in Equations (1)–(5) is combined with the user material subroutine (UMAT) in the FEM software ABAQUS/Standard, and the SMA material parameters are defined by this UMAT, where the material parameters of SMA (Ni51Ti49 (at. %)) are shown in Table 1.

**Table 1.** SMA ($Ni_{51}Ti_{49}$ (at. %)) material parameters.

| Parameter | Value | Parameter | Value |
|---|---|---|---|
| $E_a$ | 200 (GA) | $E_m$ | 70 (GA) |
| $\rho$ | 6500 (kg/mm3) | $C_A$ | 14 (MPa · °C) |
| $C_M$ | 8 (MPa · °C) | $A_s$ | 57.85 (°C) |
| $A_f$ | 72.85 (°C) | $M_s$ | 23.85 (°C) |
| $M_f$ | 55.85 (°C) | | |

The relationship between SMA shear strain and temperature during the heating-induced shape memory effect phase is shown in Figure 2. SMA temperature from 20 °C to 100 °C in the process of increasing the SMA shear strain gradually reduced to 0%. In the SMA shear strain and temperature curve there are two inflection points, and the tangential extension of the curve is formed by the virtual intersection of $A_s$ and $A_f$, The martensite to austenite transformation starts at a temperature $A_s$ of 57.85 °C. The martensite to austenite transformation finishes at a temperature $A_s$ of 72.85 °C.

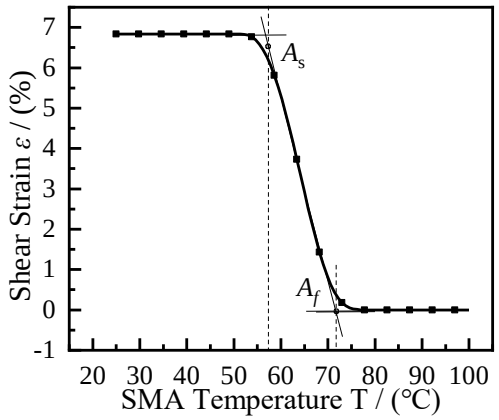


**Figure 2.** SMA shear strain versus temperature.

The simplified model for FEM is established as shown in Figure 3. In Figure 3b, the wire diameter of the SMA spring $d$ = 1.95 mm, the helical angle of the spring coil $\alpha$ = 6°, spring diameter $D$ = 12.5 mm ($D = 2R$), free height $L_0$ = 20 mm, and effective number of helical turns $n_e$ = 6. A simplified SMA fan clutch model is shown in Figure 3a, where $R_1$ = 110 mm, $R_2$ = 100 mm, $R_3$ = 70 mm, $L_1$ = 28 mm, and $L_2$ = 20 mm. Meanwhile, except for the friction ring, which is a semi-metallic friction material, all the other parts are set to Q235, and the friction coefficient between the contact parts is $\mu$ = 0.35. When the load is set by FEM, the rotor is set as displacement constraint, the friction ring is set as fixed constraint, the initial temperature $T_0$ of SMA spring is set as 25 °C, and $T$ is set as 100 °C when heating.

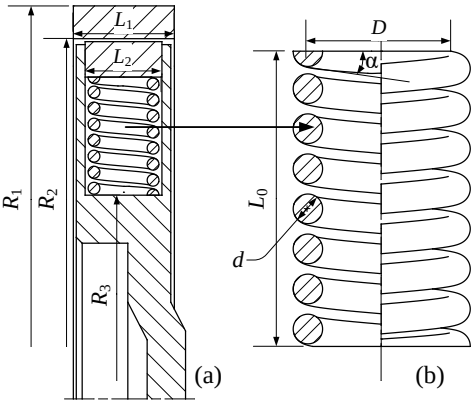


**Figure 3.** FEM analysis simplified model. (**a**) Schematic diagram of simplified model; (**b**) Simplified spring model.

The stress distribution cloud of the SMA fan clutch analyzed by FEM is shown in Figure 4. To observe the stress distribution of the SMA fan clutch, the stress distribution of the SMA spring is not shown in Figure 4, because the stress produced by the shape memory effect of SMA spring heating is much greater than the contact stress in the device. The stress distribution during the SMA spring shape memory effect is shown in Figure 5.

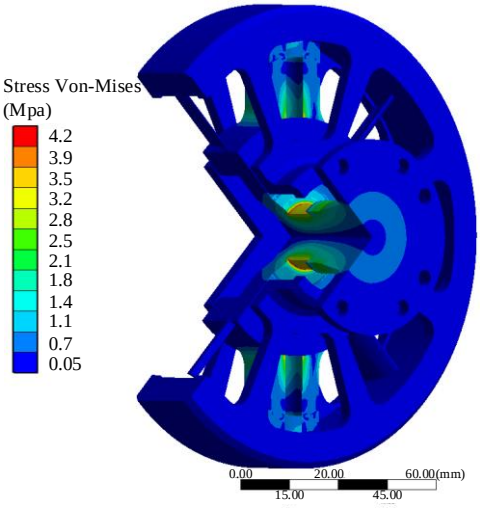


**Figure 4.** SMA fan clutch stress distribution.

The results of FEM analysis show that the maximum recovery force $F_r$ of the SMA spring is 68 N when the temperature of SMA reaches 100 °C. When the friction ring rotates counterclockwise, the contact stress of the slider will be concentrated on both sides. The maximum stress value at the contact point between the friction ring and the slider is 1.42 MPa. Since the FEM takes into account the elastic deformation of the material, the friction torque calculation method is more accurate than that shown in Equation (15). The friction torque generated by a single SMA spring by the FEM is 2.514 N·m.

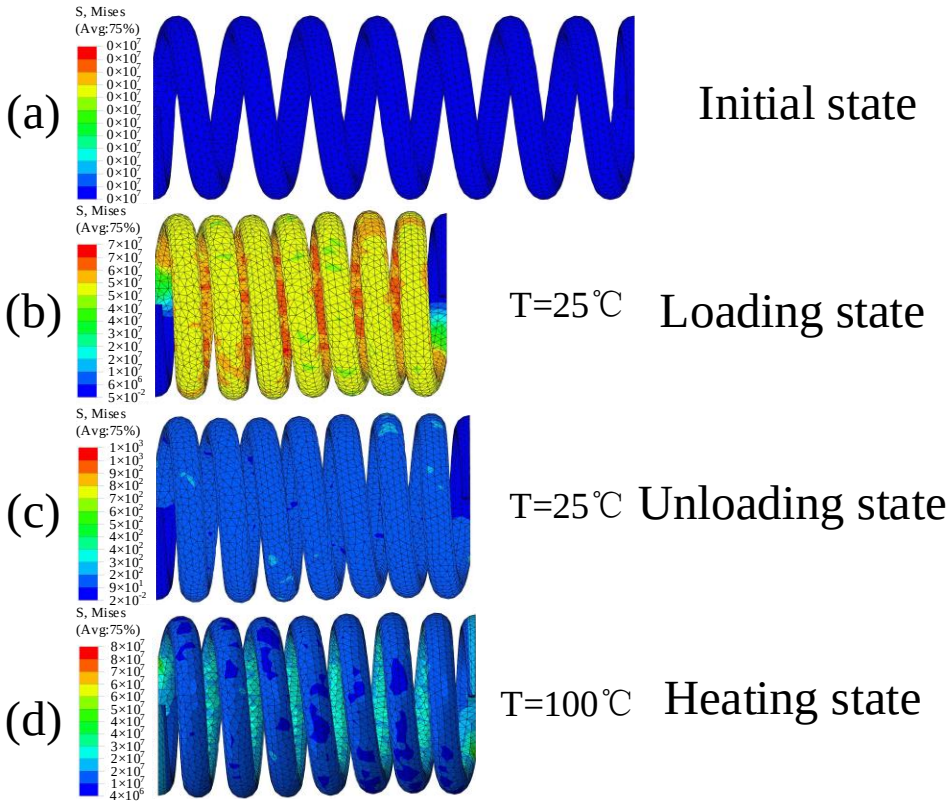


**Figure 5.** SMA stress distribution plots for each state. (**a**) Initial state of spring; (**b**) Loading state of spring; (**c**) Unloading state of spring; (**d**) Heating state of spring.

The stress distribution of the SMA spring derived from the finite element analysis is shown in Figure 5. The spring invariance and stress generation in the non-initial state is

shown in Figure 5a. Figure 5b shows that when the spring is compressed during the loading phase at 25 °C, the stress in the ground flat part of the spring at both ends is small and the stress in the rest of the spring reaches a maximum value of 66.5 MPa when the SMA spring stress–strain reaches its maximum value. A partial reduction in spring compression under the unloading phase is shown in Figure 5c, while the SMA spring stresses are all reduced to 0 MPa and the maximum residual strain $\varepsilon_L$ generated by the SMA is 6.5%. The SMA generates a shape memory effect in the heated condition, and the SMA spring stress increases and generates a return force $F_r$ to the bottom of the slider because the SMA spring end face is constrained by the axial displacement of the slider against it, as shown in Figure 5d.

The stress–strain curves during the generation of shape memory effect in the SMA, as simulated by the FEM, are shown in Figure 6. The nonlinear stress caused by the external force load ($F$ = 80 N) during the loading phase increased to 66.5 MPa, at which time the nonlinear strain generated by the SMA was 7.6%. After completing the loading, the SMA transforms from austenite to non-twin martensite, the external load is withdrawn, and the SMA enters the unloading stage, where the nonlinear strain can be recovered during the stress reduction to 0 MPa to transform into residual strain, which is 6.8% at this time ($\varepsilon = \varepsilon_L$). Finally, by heating the SMA temperature to 100 °C, the SMA transforms from non-twin martensite to austenite, and the residual strain is not recovered because the axial displacement receives restraint, and the stress increases to 62.5 MPa.

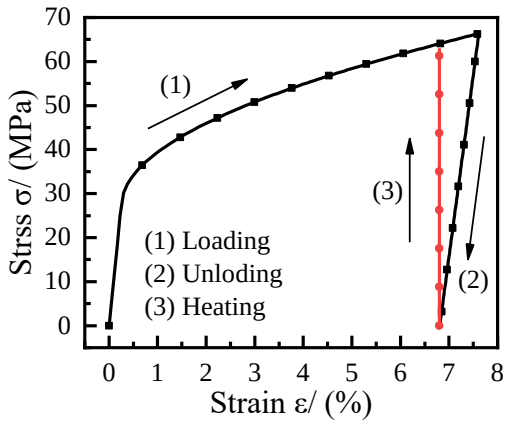


**Figure 6.** Stress–strain curves of SMA in different states.

## 5. Experiment

The SMA spring thermal drive performance test setup is shown in Figure 7, which tests the relationship between temperature and recovery force of SMA springs under the shape memory effect.

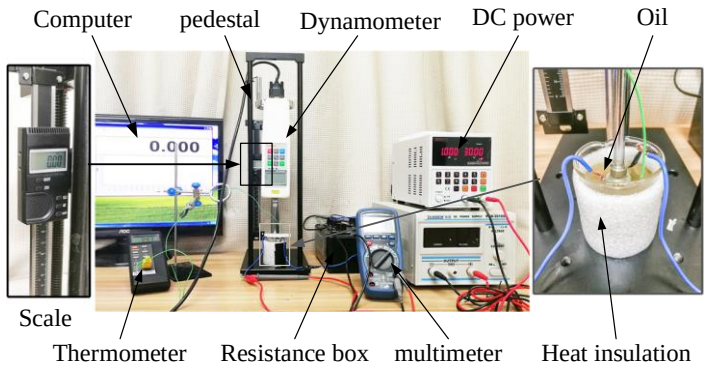


**Figure 7.** SMA spring thermal driving performance test.

The main devices involved in this setup include a digital display push–pull meter, digital display thermometer, manual base, digital display scale, and digital DC power supply. The gap between the SMA spring and beaker inner wall is filled with hydraulic oil (specific heat capacity: 1.7 KJ/(kg °C), heat transfer rate: 0.2 W/(m °C)). The hydraulic oil has good heat transfer, and while the thermocouple is in contact with the SMA surface, the hydraulic oil in the gap between the thermocouple and SMA conducts the heat from SMA to the thermocouple by heat transfer, which can improve the accuracy and stability of the SMA temperature measurement.

During the test, heat is generated by energizing the wire, the temperature of the SMA surface is recorded by a digital thermometer, and the response force generated by the SMA spring is recorded by a force gauge.

The relationship between the SMA spring reversion force and temperature is shown in Figure 8. The temperature curves of the experimentally derived restoring force are consistent with the theoretically calculated restoring force temperature curves. When the SMA spring temperature is lower than 45 °C, the growth of the recovery force $F_r$ is slower. When the temperature of the SMA spring is between 45 °C and 80 °C, the growth of $F_r$ is more rapid. When the SMA spring temperature exceeds 95 °C, the growth of the $F_r$ tends to stagnate, and the $F_r$ reaches a maximum when the SMA spring temperature reaches 100 °C. The experimental maximum $F_r$ is 66.3 N, and the maximum $F_r$ based on the FEM is 68.1 N, with an error of 2.71%.

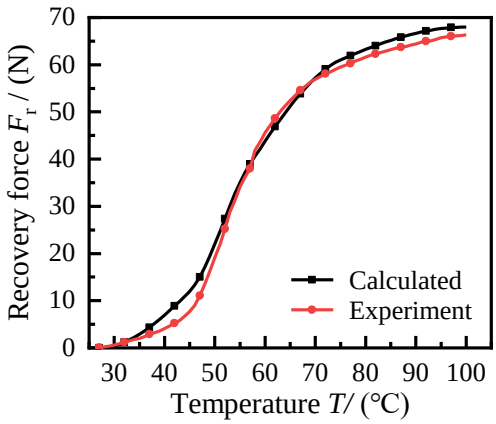


**Figure 8.** SMA spring reversion versus temperature curves.

The relationship between SMA spring temperature and friction torque can be obtained by combining the friction torque calculation formula shown in Equation (11) and the SMA spring return force versus temperature shown in Figure 8, as shown in Figure 9. The maximum torque that can be transmitted by the clutch is 9.52 N·m ($T$ = 100 °C) when the number of SMA springs inside the clutch is four (N = 4), and 19.04 N·m ($T$ = 100 °C) when the number of SMA springs is eight (N = 8). Considering the wide circumferential SMA spring-mounting position of the adaptive SMA fan clutch, as shown in Figure 1, two SMA spring arrangement schemes were designed, one with four SMA springs evenly distributed around the rotor and the other with eight SMA springs around the rotor. With different SMA spring arrangements, different transmission characteristics can be met with the same overall structure.

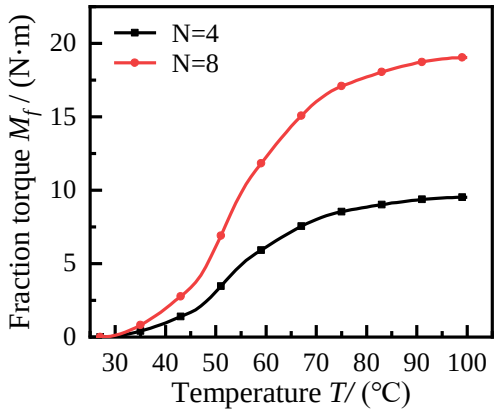


**Figure 9.** SMA spring temperature and friction torque curves.

To illustrate the superior performance of this intelligent fan clutch, it is compared with the F450 type fan clutch, a 103 kW LR6ALR22/1030 supercharged engine radiator with a matching F450 fan diameter $D$ of 450 mm, combined with the fan torque speed calculation formula shown in Equation (12), where the torque coefficient in air $K_a$ is 0.96 and air density $\rho$ is 1.293 kg/m$^3$ while assuming a constant clutch input speed $n_0$ of 3000 rad/min. The calculated fan torque versus speed is shown in Figure 10. It can be seen from the figure that when the load torque increases, the fan speed growth rate gradually decreases; when the fan speed is 3000 rad/min, the corresponding load torque is 20.7 N·m.

Combining Equation (11) and the relationship between SMA spring temperature and friction torque shown in Figure 9, the maximum speed that the SMA fan clutch can transmit at different temperatures is derived, where the relationship between clutch temperature and maximum speed is shown in Figure 11.

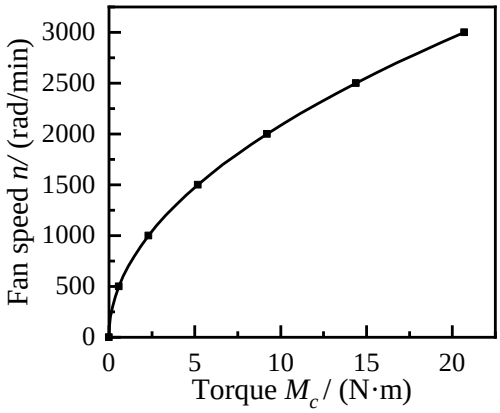


**Figure 10.** Torque versus rotation curves of SMA clutch.

From Figure 11, it can be seen that when the SMA fan clutch temperature is lower than 70 °C, the temperature and fan speed are close to linear growth, and when the SMA fan clutch temperature is higher than 75 °C, the fan speed grows more slowly as the temperature rises. When the number of SMA springs is four (N = 4), the maximum speed of the fan clutch is 2034.8 rad/min, and when the number of SMA springs is eight (N = 8), the maximum speed of the fan clutch is 2877.2 rad/min.

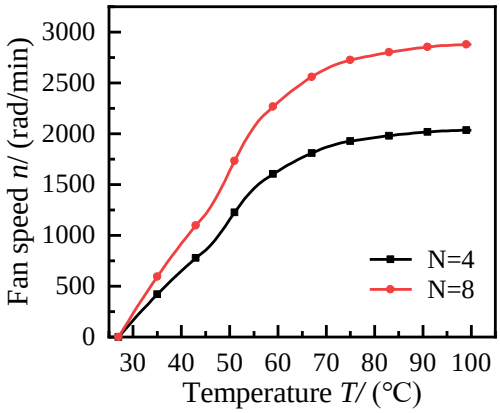


**Figure 11.** Fan speeds at different temperatures.

The synchronization characteristics of the active and driven parts of the SMA fan clutch at different temperatures are quantified by the slip ratio $S_n$, which is $S_n = (n_0 - n)/n_0$, where $n_0$ is the speed of the active part of the clutch and $n$ is the speed of the driven part. Combined with the fan speed at different temperatures of the clutch, shown in Figure 11, to obtain the slip ratio $S_n$ of SMA fan clutch at different temperatures, there is a high slip ratio $S_n$ shown in Figure 12, when the SMA fan clutch temperature is lower than 55 °C, but the slip ratio decreases more rapidly in the process of temperature increase. When the SMA fan clutch temperature is higher than 75 °C, the slip ratio $S_n$ tends to stabilize. Four SMA fan clutches are set in the SMA fan clutch in this case; the active and driven parts are not synchronized, and the relative friction is more violent during the working process, so the SMA fan clutch with four SMA springs is not suitable for driving the F450 fan. When the SMA fan clutch has eight SMA springs and the clutch temperature reaches 100 °C, the rotation rate is stabilized at 4.3%, and the active and driven parts are synchronized; at this time the SMA fan clutch can meet the required transmission performance of the fan.

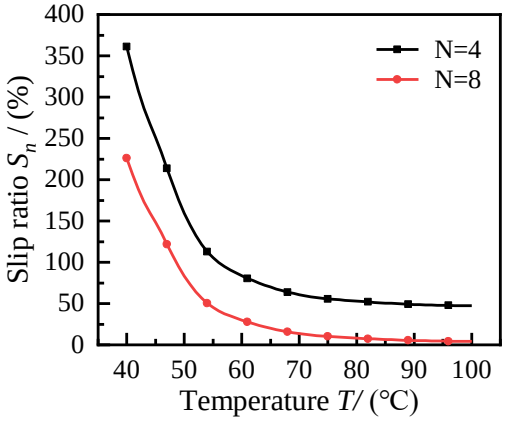


**Figure 12.** Slip rate of SMA fan clutch.

Some of the significant performance parameters of clutches used in some prevalent large hybrid vehicle drivetrains are shown in Table 2. The SMA fan clutch has certain advantages over the more common (electronically controlled) silicone oil fan clutch and electromagnetic fan clutch. First of all, the SMA fan clutch is simple and compact, and the SMA spring is the driving mechanism to transmit torque at a low rate of torque difference. Moreover, the SMA fan clutch does not need a control device, and relying on the physical characteristics of SMA, the SMA fan clutch can work continuously and steadily under the harsh conditions of large combine harvesters and other applications. Meanwhile, the SMA fan clutch analyzed in this paper with SMA ($Ni_{51}Ti_{49}$) as an example has a lower response

temperature and a wider temperature sensing range. In actual use, the ratio of Ni–Ti can be adjusted according to the working conditions and based on the programmability of SMA, so that the SMA fan clutch temperature sensing characteristics ($M_s$, $M_f$, $A_s$, $A_f$) can achieve the ideal working performance.

**Table 2.** Fan clutches performance contrast.

| | SMA Clutch | Silicone Oil Clutch [25] | Electromagnetic Clutch [26] |
|---|---|---|---|
| Slip ratio | 4.3% | 3.8% | 0% |
| Torque | 19.1 N·m | 10.8 N·m | 24.5 N·m |
| Radius | 100 mm | 120 mm | 82 mm |
| Number of parts | 7 | 9 | 11 |

## 6. Conclusions

A novel intelligent SMA fan clutch for large hybrid vehicle engines is proposed. Due to the introduction of SMA, a smart material, the clutch has a compact structure and high energy density and can work continuously and stably in a harvester with complicated road conditions.

Based on the SMA thermodynamic constitutive model in pure shear mode and the geometric equations of the helical spring, the relationship between SMA spring return force and temperature is established, and the clutch torque transfer equation is combined with the geometry of the intelligent SMA fan clutch structure. Based on the fan torque speed curve, the relationship between clutch temperature, torque, and speed is derived.

The experimental results verify the accuracy of the theoretical model and quantitatively analyze the SMA fan clutch transmission characteristics in terms of temperature, torque, rotational speed, and slip rate. The results show that the output torque is 19.04 N·m, the speed is 2877.2 rad/min, and the slip rate is 4.3% when the clutch input speed of 3000 rad/min and the temperature is 100 °C. The clutch drive performance can meet the heat dissipation requirements.

**Author Contributions:** J.H. conceived this research; H.G. and J.H. deduced the calculation; H.G. wrote the original draft preparation; editing and review on this article was completed by R.S.; G.H. is responsible for overseeing the progress and visualization of the article. All authors have read and agreed to the published version of the manuscript.

**Funding:** The authors would like to gratefully acknowledge the National Natural Science Foundation of China (NO. 51875068, NO. 51905060), the Science and Technology Research Program of Chongqing Municipal Education Commission under Grant (KJQN201901107), Natural Science Foundation Project of Chongqing Science and Technology Commission (cstc2020jcyj-msxmX0346), and the China Postdoctoral Science Foundation (2021M700619) for their support.

**Institutional Review Board Statement:** Not applicable.

**Informed Consent Statement:** Not applicable.

**Data Availability Statement:** Not applicable.

**Conflicts of Interest:** The authors declare no conflicts of interest. The funders had no role in the design of the study; in the collection, analyses, or interpretation of data; in the writing of the manuscript, or in the decision to publish the results.

## References

1. Mohd Jani, J.; Leary, M.; Subic, A.; Gibson, M.A. A review of shape memory alloy research, applications and opportunities. *Mater. Des. (1980–2015)* **2014**, *56*, 1078–1113. https://doi.org/10.1016/j.matdes.2013.11.084.
2. Ölander, A. An Electrochemical Investigation of Solid Cadmium-Gold Alloys. *J. Am. Chem. Soc.* **1932**, *54*, 3819–3833. https://doi.org/10.1021/ja01349a004.

3. Auricchio, F.; Scalet, G.; Urbano, M. A Numerical/Experimental Study of Nitinol Actuator Springs. *J. Mater. Eng. Perform.* **2014**, *23*, 2420–2428. https://doi.org/10.1007/s11665-014-0883-1.
4. Wang, Z.G.; Zu, X.T.; You, L.P.; Feng, X.D.; Zhang, C.F. Investigation on the two-way shape memory effect and alternating current electrothermal driving characteristics of TiNiCu shape memory alloy. *J. Mater. Sci.* **2004**, *39*, 3391–3395. https://doi.org/10.1023/B:JMSC.0000026941.93740.ec.
5. Ryhanen, J.; Niemi, E.; Serlo, W.; Niemela, E.; Sandvik, P.; Pernu, H.; Salo, T. Biocompatibility of nickel-titanium shape memory metal and its corrosion behavior in human cell cultures. *J. Biomed. Mater. Res.* **1997**, *35*, 451–457.
6. Cho, H.; Suzuki, A.; Yamamoto, T.; Sakuma, T. Mechanical Behavior of Shape Memory Alloys Under Complex Loading Conditions of Stress, Strain, and Temperature. *J. Mater. Eng. Perform.* **2012**, *21*, 2587–2593. https://doi.org/10.1007/s11665-012-0317-x.
7. Spinella, I.; Dragoni, E. Analysis and Design of Hollow Helical Springs for Shape Memory Actuators. *J. Intell. Mater. Syst. Struct.* **2009**, *21*, 185–199. https://doi.org/10.1177/1045389x09356021.
8. Weirich, A.; Kuhlenkötter, B. Applicability of Shape Memory Alloys in Aircraft Interiors. *J. Actuators* **2019**, *8*, 61. https://doi.org/10.3390/act8030061.
9. Gédouin, P.-A.; Pino, L.; Arbab Chirani, S.; Calloch, S.; Delaleau, E.; Bourgeot, J.-M. R-phase shape memory alloy helical spring based actuators: Modeling and experiments. *Sens. Actuators A Phys.* **2019**, *289*, 65–76. https://doi.org/10.1016/j.sna.2019.02.024.
10. Imran, H.Y.; Majid, D.L.A.A.; Ethaib, S.; Baitab, D.M.; Jang, L.S. Utilization of Shape Memory Alloy (SMA) for Temperature Detection and Warning in an Automobile Engine. *IOP Conf. Ser. Mater. Sci. Eng.* **2021**, *1058*, 12039. https://doi.org/10.1088/1757-899x/1058/1/012039.
11. Chillara, V.S.C.; Headings, L.M.; Tsuruta, R.; Itakura, E.; Gandhi, U.; Dapino, M.J. Shape memory alloy–actuated prestressed composites with application to morphing automotive fender skirts. *J. Intell. Mater. Syst. Struct.* **2018**, *30*, 479–494. https://doi.org/10.1177/1045389x18812702.
12. Shivaram, A.C. Smart actuators to improve sportiness of a luxury car by deploying additional suspension stiffness on-demand. *Int. J. Veh. Des.* **2012**, *60*, 155–175. https://doi.org/10.1504/ijvd.2012.049162.
13. Mingye, Y.; Song, H.; Fuyuan, Y.; Liangfei, X.; Yu, B.; Dian, Y. On-Board Liquid Hydrogen Cold Energy Utilization System for a Heavy-Duty Fuel Cell Hybrid Truck. *World Electr. Veh. J.* **2021**, *12*, 136.
14. Lee, K.J.; Kang, N.; Kokkolaras, M.; Papalambros, P.Y. Design optimisation of a hybrid electric vehicle cooling system considering performance and packaging. *Int. J. Veh. Des.* **2021**, *85*, 154–177.
15. Wei, C.G.; Zhao, W.H. The Development of the Electrically Actuated Viscous Fan Clutch. *China Mech. Eng.* 2000, *10*, 112–115+9.
16. Liu, F. Engine Cooling Device of New Energy Vehicle. *J. Phys. Conf. Ser.* **2021**, *2066*, 12103. https://doi.org/10.1088/1742-6596/2066/1/012103.
17. Karimi, D.; Behi, H.; Akbarzadeh, M.; Mierlo, J.V.; Berecibar, M. Holistic 1D Electro-Thermal Model Coupled to 3D Thermal Model for Hybrid Passive Cooling System Analysis in Electric Vehicles. *Energies* **2021**, *14*, 5924. https://doi.org/10.3390/en14185924.
18. Bencs, P.; Alktranee, M. The potential of vehicle cooling systems. *J. Phys. Conf. Ser.* **2021**, *1935*, 12012. https://doi.org/10.1088/1742-6596/1935/1/012012.
19. Xu, L.; Solomou, A.; Baxevanis, T.; Lagoudas, D. Finite strain constitutive modeling for shape memory alloys considering transformation-induced plasticity and two-way shape memory effect. *Int. J. Solids Struct.* **2020**, *221*, 42–59. https://doi.org/10.1016/j.ijsolstr.2020.03.009.
20. Zhou, B.; Liu, Y.; Leng, J.; Zou, G. A macro-mechanical constitutive model of shape memory alloys. *Sci. China Ser. G Phys. Mech. Astron.* **2009**, *52*, 1382–1391. https://doi.org/10.1007/s11433-009-0173-3.
21. Xiong, Y.; Huang, J.; Shu, R.Z. Combined braking performance of shape memory alloy and magnetorheological fluid. *J. Theor. Appl. Mech.* **2021**, *59*, 355–368. https://doi.org/10.15632/jtam-pl/136346.
22. Ma, J.Z.; Huang, H.L.; Huang, J. Characteristics Analysis and Testing of SMA Spring Actuator. *Adv. Mater. Sci. Eng.* **2013**, *2013*, 823594. https://doi.org/10.1155/2013/823594.
23. Xiong, Y.; Huang, J.; Shu, R. Thermomechanical performance analysis and experiment of electrothermal shape memory alloy helical spring actuator. *Adv. Mech. Eng.* **2021**, *13*, 1–12. https://doi.org/10.1177/16878140211044651.
24. Chen, W.; Huang, J.; Yang, Y. Research on the Transmission Performance of a High-Temperature Magnetorheological Fluid and Shape Memory Alloy Composite. *Appl. Sci.* **2022**, *12*, 3228. https://doi.org/10.3390/app12073228.
25. Yin, Z.; Zhao, K.; Shangguan, W.; Song, L. Analytical and experimental characterization of viscous fan clutch performances including thermal dynamics. *Proc. Inst. Mech. Eng. Part C J. Mech. Eng. Sci.* **2016**, *231*, 876–891. https://doi.org/10.1177/0954406215619448.
26. Lee, M.H.; Kim, M.K.; Park, H.G.; Lee, K.S.; Chun, H.H. Electronically controlled viscous cooling fan clutch in the vehicle. *Int. J. Precis. Eng. Manuf.* **2011**, *12*, 983–992. https://doi.org/10.1007/s12541-011-0131-7.